CERN Summer Student Report

Characterization of single-diode silicon sensors for the CMS HGCAL project

Report by:

Jenan Amer, An Najah National University, Palestine

Supervisors:

Leena Diehl, CERN, Geneva, Switzerland
Oliwia Kałuzińska, CERN, Geneva, Switzerland

August 18, 2023

Abstract

CERN alongside other institutes is currently in the process of testing silicon sensors for the High Luminosity upgrade of the Compact Muon Solenoid (CMS). These silicon sensors will be used for the high-granularity calorimeter (HGCAL), which is set to replace CMS's end cap calorimeter. HGCAL will utilize silicon 8-inch hexagonal silicon sensors, however, single diode test structures are produced alongside the full sensors for further research. Both need to undergo electrical characterization before and after irradiation; to study the effect of that on their functionality. This report focuses on the electrical characterization procedures and results obtained from a campaign led on neutron-irradiated single diode test structures during the period June–August of 2023 by performing temperature scans.

Contents

1 Introduction

The Standard Model represents our best understanding of how the fundamental particles and fundamental forces are related to each other. The fundamental particles are divided into fermions and bosons. Fermions are the basic building blocks of matter and are further divided into two basic types called quarks and leptons. Bosons are what we call force carriers. Three of the fundamental forces result from the force-carrier particles. They are the strong, the weak, and the electromagnetic forces. The gravitational force is a mystery that is yet to be understood.

The European Organization for Nuclear Research (CERN) - first established in 1954, houses the world's largest particle accelerator, the Large Hadron Collider (LHC). It was built to explore the fundamental structure of the universe, bringing nations together through science and training the scientists through educational programs at many levels. The LHC compound houses a number of particle physics experiments, that aim to deepen our understanding of the standard model and achieve new discoveries. The four main experiments at the LHC are:

- A Toroidal LHC ApparatuS - ATLAS.
- Compact Muon Solenoid - CMS.
- A Large Ion Collider Experiment - ALICE.
- Large Hadron Collider-beauty - LHC-b.

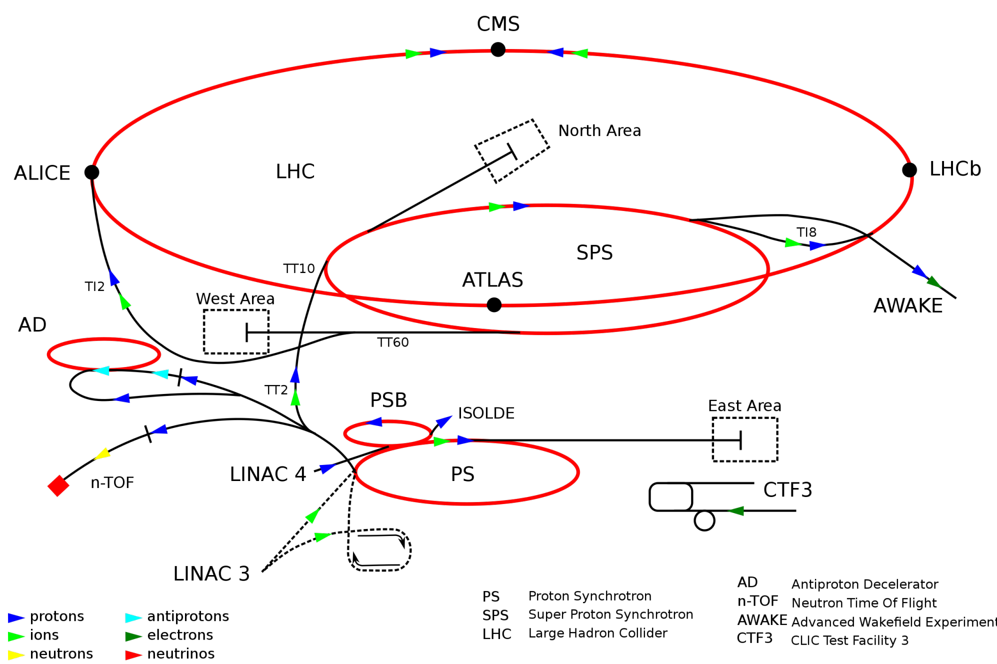

Figure 1: Schematic layout of the Large Hadron Collider Complex

Both ATLAS and CMS are general-purpose detectors, that were built to investigate a wide range of physics, including the search for the Higgs boson - which was first discovered back in 2012, extra dimensions, super-symmetry, and particles that could make up dark matter. ALICE is a specialized detector that is concerned with heavy ion collisions, mainly Pb-Pb and p-Pb. LHC-b is also a detector that specializes in investigating the slight differences between matter and antimatter by studying a type of particle called the "beauty quark", or "b quark". The four main detectors are shown in figure 1 at the main interaction points in the LHC complex. [1]

Inside the LHC ring, the number of events per cm^2 per second for a certain process can be determined by the instantaneous luminosity $\mathcal{L}_0$. For a specific number of bunches, N_b , and particles per bunch in each beam, n_i, the instantaneous luminosity is given as: [2]

$$\mathcal{L}_0 = \frac{r}{4\pi}\frac{N_b f n_1 n_2}{\sigma_x \sigma_y} \tag{1}$$

where f is the revolution frequency, and σ_i are the transverse beam dimensions in the $x-$ and $y-axis$. The reduction factor, r, which is about 0.8 for the LHC. The interaction rate, R, for a given physics process can be determined from the instantaneous luminosity and the cross-section, $_\sigma$, for that process using eqn 2.

$$R = \mathcal{L}_0 \sigma \tag{2}$$

Currently, we have about 40 collisions per beam crossing. This is set to change as the LHC is undergoing the upgrade to the High Luminosity LHC (HL-LHC). The number of collisions will be increased to about 200 collisions per bunch crossing, this will affect the LHC complex experiments. In this report, my main focus is the CMS experiment. More precisely the end-cap calorimeter of it. As the number of collisions is increased, the calorimeter along with many other detector parts needs to be upgraded in order to cope with the new challenging conditions of the HL-LHC.

2 CMS and the High Granularity Calorimeter (HGCAL)

CMS is a general-physics detector, in principle, it works as a high-speed giant camera, that captures the collisions that occur inside it in 3D. It mainly aims to measure all stable particles that emerge from the primary interaction at the center of the collision. CMS is a very compact detector compared to ATLAS, it is 21.6 meters long and has a diameter of 14.6 meters, and its total weight is $14,000$ tons. It was specifically built to detect muons; at the heart of the CMS detector is a superconducting solenoid that produces a magnetic field of $4T$. [3]

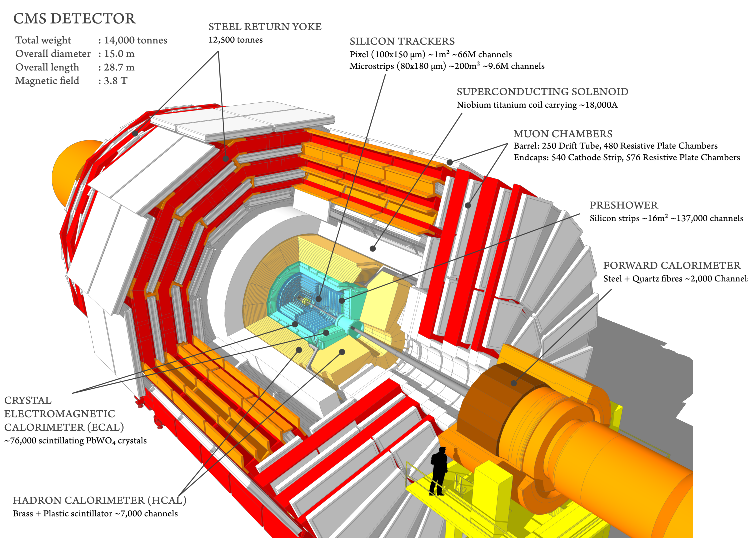

Figure 2: The CMS detector overview

The detector is composed of multiple layers, and each of the layers is designed for a specific task. The innermost part of the detector called the tracking system, is made up of silicon pixel and silicon strip sensors. They surround the interaction point at the center of the detector; they are chosen to be in this location because of their well-known radiation hardness and good position resolution. The other layers of it are the Electromagnetic Calorimeter (ECAL) and the Hadronic Calorimeter (HCAL). The first is designed to measure the trajectory and energy of particles such as photons and electrons, while the latter measures hadrons such as protons, neutrons, and pions. These calorimeters and the tracking system are placed within

the solenoid. The magnetic field generated by it bends the trajectory of these particles each to a degree depending on their momentum. [3]
As the LHC is undergoing an upgrade to higher energies, some of the CMS detector parts need to be changed to be compatible with the new, harsher conditions. The End-cap calorimeter is set to be replaced with a new high-granularity calorimeter (HGCAL), which is composed of a combination of active detector layers, namely silicon sensors and scintillators (Si) and passive absorbers (Pb, Cu).

2.1 The HGCAL upgrade Criteria

The new HGCAL has to meet very specific upgrade criteria to be compatible with the new conditions inside the LHC. These criteria are listed below:

- **Precision Measurements**, it is imperative for the HGCAL to acquire precise timing information from each cell, enabling the precise identification of vertices associated with triggering interactions.
- **Fine Lateral Granularity**, the HGCAL's signal-to-noise ratio must permit MIP (Minimum Ionising Particle) calibration. This capability aids in the differentiation of two separate showers and facilitates the observation of narrow jets.
- **Fine Longitudinal Granularity**, the system should offer a meticulous sampling of the longitudinal development of showers. This characteristic leads to excellent electromagnetic (EM) energy resolution and enhances pattern recognition.
- **Dense Calorimeter**, the HGCAL should maintain the compactness of showers in the lateral dimension. This attribute contributes to the accurate reconstruction of particle energies.
- **Radiation Tolerance**, the HGCAL must retain energy resolution even after exposure to the equivalent of 3000 inverse femtobarns (fb-1) of integrated luminosity. This preservation is contingent on effective inter-cell calibration, with a tolerance of (3%).
- **Decision Making**, the new HGCAL should play a role in the level-1 triggering process, contributing to the system's decision-making capabilities.

2.2 Structure of the HGCAL

The HGCAL will cover a pseudorapidity range from 1.5 to 3, it will have a mass of 215 Tonns per end cap, a full system maintained at - 30^oC. An area of $620m^2$ will be covered with silicon sensors, consisting of approximately 26000 modules. It will have 6 Million Si channels with cell sizes of $0.6cm^2$ or $1.2cm^2$. The scintillators will also have an area of about $370m^2$ in 3700 boards. We will have $240k$ scintillation channels with cell sizes $4 - 30cm^2$.
We will have three different thicknesses- $120\mu m$, $200\mu m$, and $300\mu m$ of silicon sensors inside the HGCAL, distributed depending on the expected radiation damage corresponding to the location with respect to the interaction point at the center of the detector. Sensors with lower thicknesses have much higher density and smaller cell sizes. The $120\mu m$ sensors will be placed at the inner part of the HGCAL, while the $200\mu m$ and the $300\mu m$ sensors will be placed on the outer parts, this is shown in figure 3.

3 Silicons Sensors

3.1 Why do we use silicon sensors?

Silicon sensors are the foundation of what we call solid-state detectors. Solid-state detectors are radiation detectors that employ a semiconductor material (Si) as the detecting medium. They are very well known for their radiation hardness, extremely precise measurements, high readout speed, the simultaneous measurement of energy, position, and arrival time, and the possibility of integrating the detector and the readout electronics on the same substrate.

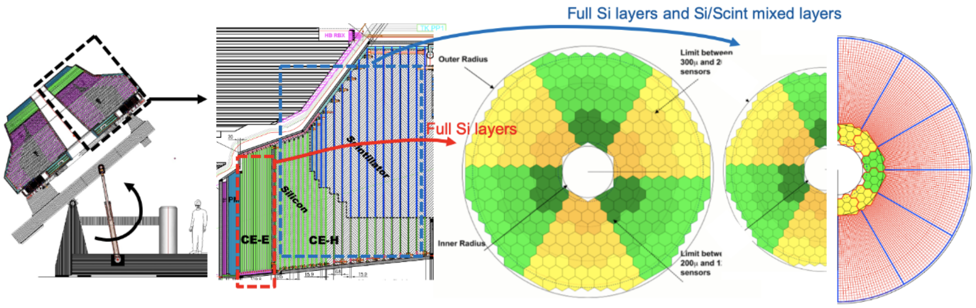

Figure 3: Design of the HGCAL, to the left we have a Sketch of the HGCAL endcap, on the mid-left we see the internal structure on the longitudinal-radial (z-r) plane. Red and blue rectangles indicate regions of CE-E and CE-H respectively, where CE-E has 28 full Si layers and CE-H has 8 full Si layers plus 14 Si-scintillators hybrid layers. Mid-right, Right: Layouts of CE-E and CE-H layer. Silicon wafers are shown as yellow and green hexagons and scintillators are shown as red mesh. Darker, medium, and lighter shades of hexagons represent silicon wafers with thicknesses of 120, 200, and 300 μm respectively.

3.2 How do silicon sensors work?

- When charged particles pass through a silicon strip, they create electron-hole pairs through ionization. An electric field guides the charge carriers (e and h) towards positive and negative electrodes.
- Charge carriers induce signals in nearby strips proportional to the deposited energy. Measuring signal times and amplitudes determines the particle path with precision. The activated strip pattern gives trajectory measurements.
- Electronic circuits read signals, amplify them, and convert them to digital data.
- Combining data from multiple detector layers reconstructs the charged particle's 3D path, which is vital for understanding interactions and particle properties. [4]

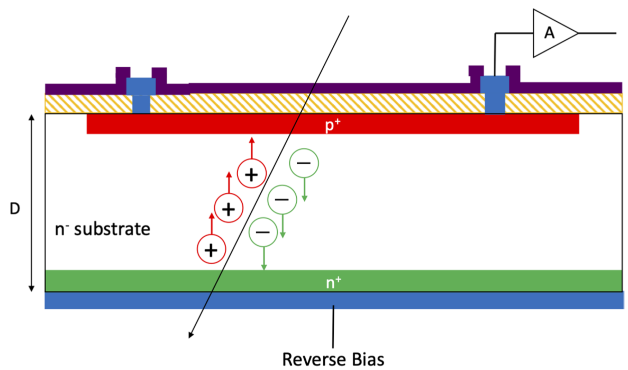

Figure 4: Operation principle of a silicon radiation detector.

3.3 Silicon sensors for HGCAL

The silicon sensors for HGCAL are manufactured as geometrical 8-inch circular wafers, these wafers are then cut into hexagonal shapes; This shape is chosen for the most effective use of the area. Each sensor is segmented into hundreds of cells or pads which are also of hexagonal shape. The diodes for HGCAL are "n-in-p" type, they are produced in three different thicknesses, 300 μm, 200 μm and 120 μm. [5]
The 300 and 200 μm sensors are fabricated using the float zone method. They are made from 600 μm wafers which are thinned to target thickness on the backside after front-side processing. The 120 μm sensors

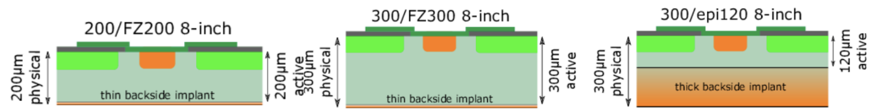

Figure 5: Sensors cross section for the three different thicknesses: 300, 200 and 120 μm

are produced in the epitaxial process. They have a thick substrate wafer of around 180 μm, on which the epitaxial wafer is grown. Figure 5 shows a cross-section of the three different sensor thicknesses.
The hexagonal sensors, that are cut out from the hexagonal wafers along with some test structures, are what we call full sensors, and they could have either high or low density of cells. The diode test structures are placed in the spaces around the hexagonal cut in the shape of half moons. This is all shown in figure 6. The diode test structures in the half moons are labeled by their position on the wafer. They are labeled as upper left (UL), upper right (UR), lower left (LL), and lower right (LR).

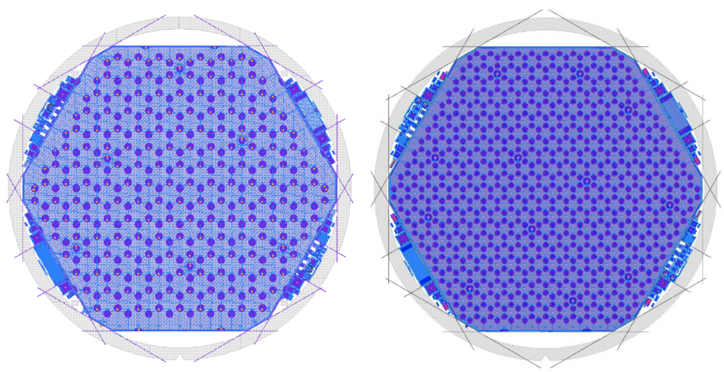

(a) (b)

Figure 6: Sensor designs for HGCAL: (a) low and (b) high-density layout. Both wafer layouts include the main hexagonal sensor and four half-moons containing test structures

4 Measurement and analysis of single-diode test structures

4.1 Introduction and motivation

The full sensors and the diode test structures need to pass specific criteria to be deemed good for use. One can verify the quality of the sensors by performing electrical characterization measurements on the sensors. This type of study is done before and after irradiation of the sensor so we can predict the effect of the high radiation doses in the detector. Our study focused on the electrical characterization of neutron-irradiated diode test structures mentioned in the previous section through current-voltage (IV) and capacitance-voltage (CV) measurements. We have a set of pre-series and pre-production irradiated single diodes that were the subject of our studies for the past two months. The study focused on the effect of changing the temperature on the CV and IV measurements.

4.2 Experimental setup and electrical characterization procedures

The setup we used to perform our measurements is the CERN EP-DT-DD group probe station. It is composed of a Faraday cage that encloses the test area, protects it against electromagnetic radiation, and minimizes the amount of light coming to the DUT (Device Under Test). Inside the cage, we have a temperature-controlled chuck on which we place the DUT. The DUT in our case is the small diode test structures. It's fixed to the chuck with vacuum suction. Once the placement of the DUT is correct we can then establish contact with the sample. This is done with two needles at two specific locations, one at the guard ring

of the diode test structure while the other makes contact at the test structure's pad for signal reading. A microscope is used to visualize the test structures while establishing the contact. Once the contact is done we can close the Faraday cage and flush the area with dry air; this is to control the humidity around the sample when testing.
The temperature on the chuck and the sample is controlled with a chiller unit. Our measurements are done at temperatures between -30 and $-12^{o}C$. We chose such low temperatures since the diodes are heavily irradiated and have very high leakage currents.

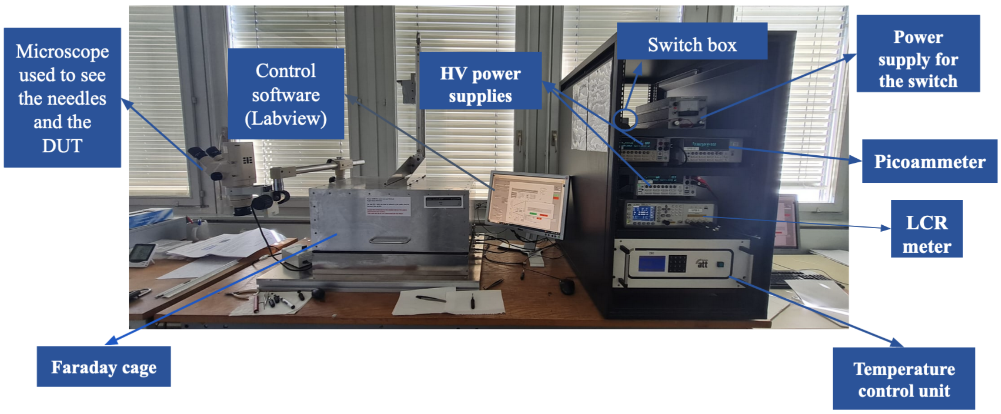

Figure 7: CERN EP-DT-DD group probe station

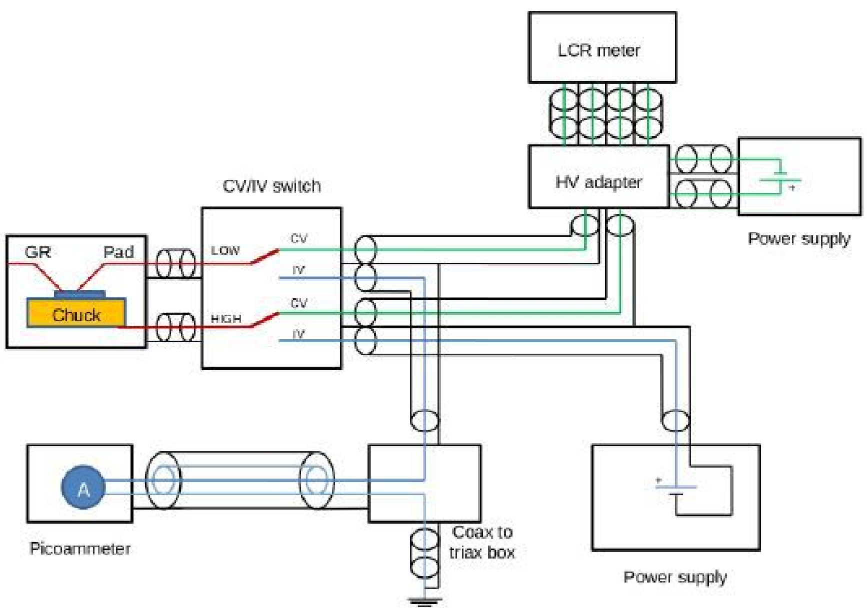

Figure 8: CERN EP-DT-DD SSD group probe station schematic

Figure 8 shows a schematic of the setup in figure 7, it shows all the parts of the IV/CV probe station. For the IV part, the high voltage is provided by a power supply - Keithley 2410. Leakage current is measured by a picoammeter - Keithley 6487. While for the CV part, the same type of device is used as a high-voltage source -Keithley 2410, the readout of capacitance is done by an LCR meter - Keysight E4980A. The CV measurement is done by applying DC bias voltages on the sensor while making the measurements with an AC signal. For all our measurements on the diode test structures, we use a frequency for the AC signal of $2kHz$. The setup combines IV and CV measurements in one setup by using a high-frequency switch- H6P-330127, which enables the automatic switching between the two types of measurements.

4.3 Temperature scans of single diodes

Temperature scans were performed on a collection of neutron-irradiated pre-series single diodes with the aim of studying the effect of changing the temperatures on parameters like the leakage current and the depletion voltage. We have three different thicknesses of diodes (120, 200, and 300μm) that were irradiated in June of 2023 at Jozef Stefan Institute (JSI) to Fluences up to 1.5e16 n_{eq}/cm^2. Table 1 shows a list of the diodes irradiated. We note that not all of them were subject to temperature studies.

Table 1: List of single diodes irradiated at Jozef Stefan Institute (JSI) in June 2023

Thickness (μm)	Fluence (n_{eq}/cm^2)	Number of diodes
300	2e15	6 (pre-series) + 4 (pre-production)
300	4e15	6 (pre-series) + 6 (pre-production)
200	4e15	6 (pre-series)
200	6e15	5 (pre-series)
200	8e15	4 (pre-series)
120	6e15	6 (pre-series)
120	1.5e16	6 (pre-series)

Temperature scans are done for capacitance-voltage (CV) and current-voltage (IV) measurements at different temperatures. For our study, we did these scans at -30, -28, -26, -24, -22, -20, -18, -16, -14 and -12^oC.These measurements are controlled via a Lab-view-based software, a screenshot of the software is shown in figure 9.

Figure 9: Labview software screenshot while running an IV measurement

Once the DUT is placed correctly on the chuck and the area is flushed with dry air we then can start with the measurements. The temperature is first set to -20^oC which is the temperature that is typically used for the electrical characterization measurements on irradiated diodes.

4.4 CV temperature scan results

The CV measurements are typically performed at a frequency of $2kHz$. The applied voltage or the bias voltage ranges between $0V$ and $900V$. An example of the CV temperature scan can be seen in figure 10. Here we can observe the effect of the different thicknesses on the depletion of the irradiated single diodes. For the $120\mu m$ diode we reach the full depletion until the maximum bias voltage. The behavior of the depletion voltage seems to be dependent on the temperature, this can be clearly observed in Figure 11.

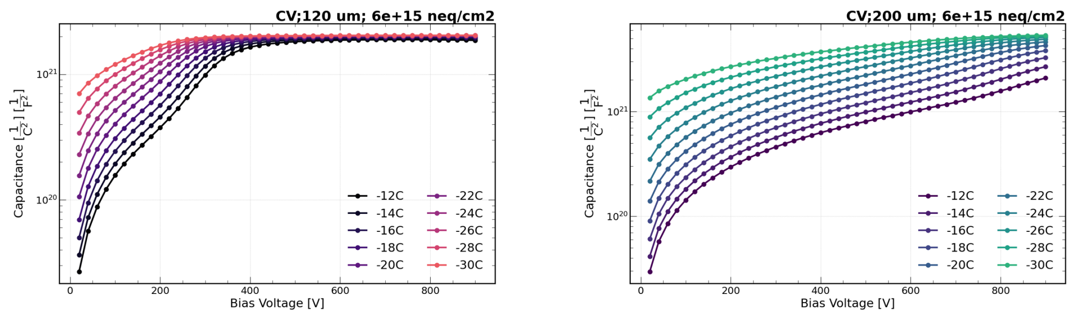

(a) CV temperature on $120\mu m$ single diode

(b) CV temperature on $200\mu m$ single diode

Figure 10: CV temperature scan results on $120\mu m$ and $200\mu m$ single diodes irradiated to $6e + 15$ n_{eq}/cm^2

This depletion is however not observed in diodes of higher thicknesses. This can be seen in Figure 10b, even though the $200\mu m$ diode is irradiated to the same fluence as the $120\mu m$ diode, it doesn't reach the full depletion until the same maximum applied voltage. The same can be said for the $300\mu m$ diode, it doesn't reach full depletion.

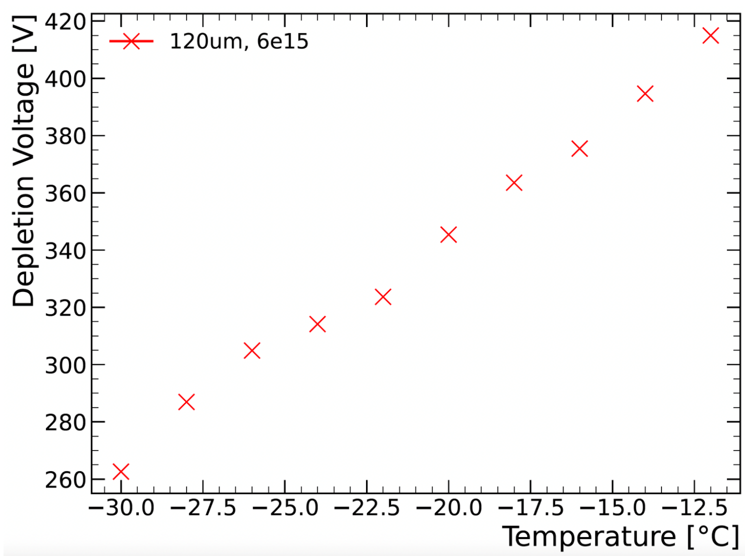

Figure 11: Depletion voltage as a function of the temperature extracted from figure 10a

4.5 IV temperature scan results

The IV measurements are also done with an applied bias voltage ranging between $0V$ and $900V$. An example of this can be seen in Figure 12. It's observed that the value of the leakage current, which is in the order of a few μA, is affected by the fluence of the irradiated diode at the same thickness. A $120\mu m$ test structure irradiated to a fluence of $1.5e16$ n_{eq}/cm^2 registers a leakage current higher than that of the test structure of the same thickness and a fluence of 6e15 n_{eq}/cm^2. It's also observed at all fluences and thicknesses of irradiated test structures that the value of the leakage current increases exponentially with an increase in temperature.

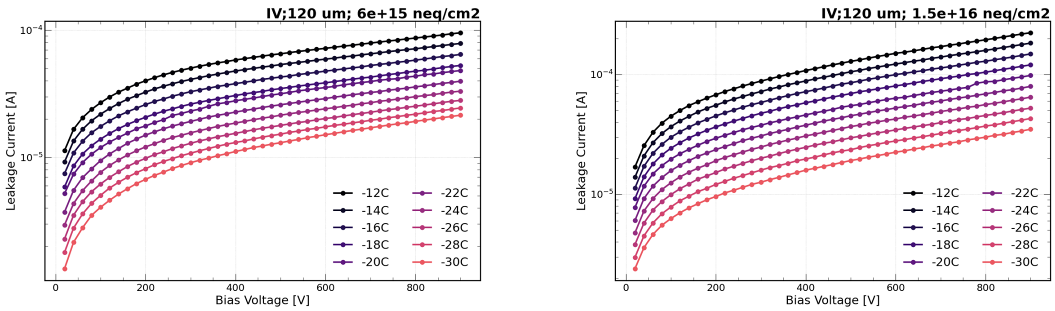

(a) Irradiated to $6e + 15\ n_{eq}/cm^2$ (b) Irradiated to $1.5e + 16\ n_{eq}/cm^2$

Figure 12: IV temperature scan results on 120μm single diodes irradiated to different fluences

4.5.1 Arrhenius plot and the activation energy

The activation energy in the context of semiconductor leakage current refers to the energy barrier that must be overcome for charge carriers (electrons or holes) to move across the semiconductor material and contribute to a leakage current. The concept of activation energy is often used to describe the behavior of leakage current in semiconductors. [6]

From the IV temperature scan results we can do an Arrhenius plot, this is a plot of the leakage current normalized with the volume of our small test structures as a function of the inverse of the temperature [7]. Figure 13 is an example of this plot. From the slope of the fit, we can then extract the activation energy. The parameter A in eqn.3 is the slope of each of the fit lines in figure 13 and it corresponds to the value of the activation energy for each of the test structures.

$$\frac{I(600V)}{V} = exp(\frac{-A}{K_B T} + B) \tag{3}$$

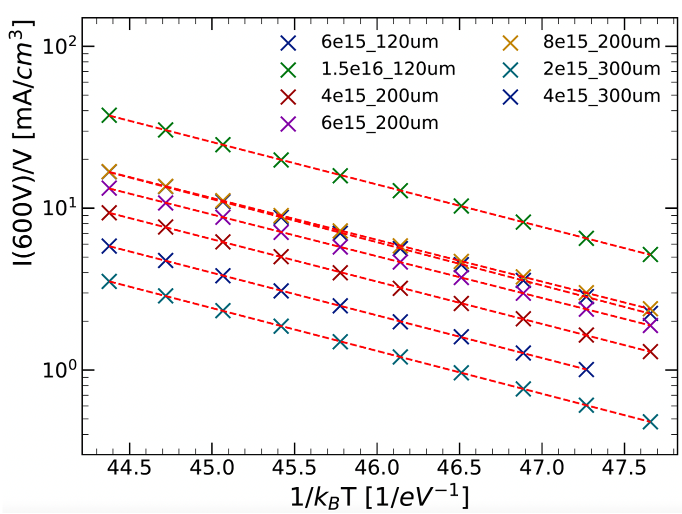

Figure 13: Arrhenius plot- volume normalized leakage current as a function of the inverse of the temperature. We note that the y-axis is in the log scale

Figure 13 shows the Arrhenius plot for a sample of the test structures tested. More of the irradiated test structures with different thicknesses and fluences were tested to investigate the dependence of the activation energy of the fluence. The slope of each of the fit lines in figure 13 is roughly the same across all measurements.

4.5.2 Activation energy and fluence dependence

Figure 14 is a plot of the activation energy as a function of the fluence. We see a large spread and uncertainty in the measurements. Given this large spread, we can't clearly state that there is a dependence of the activation energy on the fluence. It's possible that fluence dependencies may come into play only if we have a much larger range of fluences.

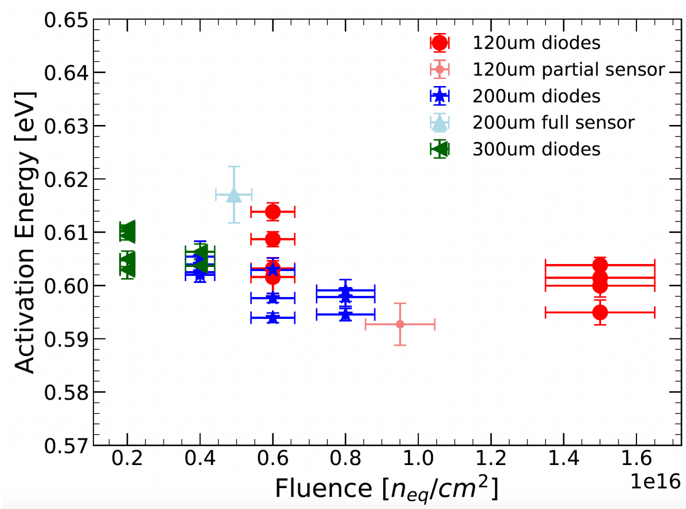

Figure 14: Activation energy vs. the fluence of the irradiated test structures

One possible reason for this large spread in the activation energy is the relatively large spread of the volume normalized leakage current over the fluences plot (Alpha plot). In Figure 15, if we compare this campaign's results to a previous campaign done in 2021 where the test structures were mounted on PCBs this spread is very apparent, and this could be one of the reasons for the spread in the activation energy. A slight difference between thicknesses for the same fluence was also observed with the old sensors.

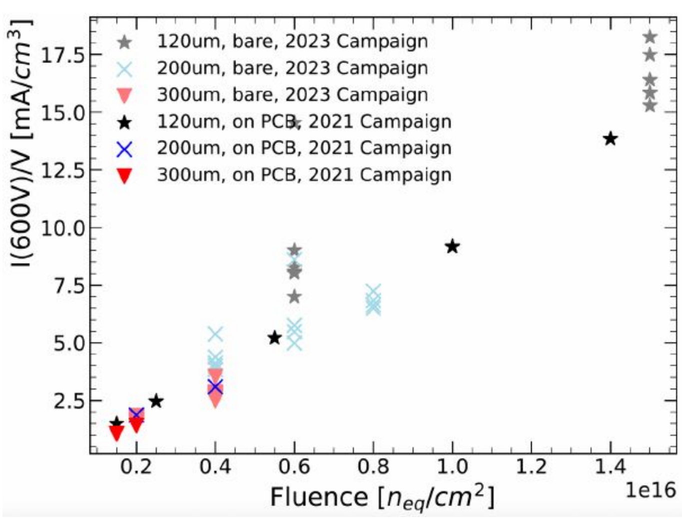

Figure 15: Volume normalized leakage current vs. the fluence of the irradiated test structures (Alpha plot)

5 Conclusion

At CERN, electrical characterization of neutron-irradiated single-diode test structures of different thicknesses and fluences using current-voltage (IV) and capacitance-voltage (CV) temperature scans was performed. The results of the CV and IV temperature scans are in agreement with what was expected, an exponential increase of current with the increase of temperatures is observed in the IV temperature scans, while a shift in the depletion voltage with temperature is noticed in the CV temperature scans, they also show that the $120\mu m$ irradiated test structures can reach full depletion until an applied bias voltage of $900V$, while the test structures of higher thicknesses $200\mu m$ and $300\mu m$ don't.
The activation energy was extracted for test structures of different thicknesses and fluences using the data from the IV temperature scans and using Arrhenius plots. A study of the dependence of the activation energy on the fluence was performed, and the results of this study showed no clear dependency of the activation energy on the fluence. It is possible that the large spread of the activation energy is related to the large spread in the Alpha plot, but this is yet to be confirmed.

References

[1] CERN. The large hadron collider. URL: "https://home.cern/science/accelerators/large-hadron-collider".

[2] B Muratori. Luminosity and luminous region calculations for the lhc. Technical report, CERN-LHC-Project-Note-301, 2002.

[3] The CMS experiment at CERN. About cms. URL: "https://cms.cern/detector".

[4] Nick Connor. What is silicon-based semiconductor detector – definition. URL: "http://www.radiation-dosimetry.org/what-is-silicon-based-semiconductor-detector-definition/#:~:text=Most%20silicon%20particle%20detectors%20work%2C%20in%20principle%2C%20by,ionization%20currents%20that%20can%20be%20detected%20and%20measured.".

[5] Oliwia Agnieszka Haluszczak. Silicon sensor characterisation and radiation hardness qualification for the cms endcap calorimeter upgrade for the high-luminosity lhc, 2022.

[6] eesemi. Activation energy. URL: "https://eesemi.com/activation-energy.htm.

[7] Vasile VN Obreja and Alexandru C Obreja. Activation energy values from the temperature dependence of silicon pn junction reverse current and its origin. *physica status solidi (a)*, 207(5):1252–1256, 2010.